Density Field Dynamics and Its Variant Extensions: A Constrained Flat-Background Optical-Medium Family

Gary Thomas Alcock

October 1, 2025

Abstract

Density Field Dynamics (DFD) reproduces all standard solar-system tests while predicting two decisive laboratory discriminators: (1) non-null cavity–atom frequency *slopes* across potential differences, and (2) a T^3 term in matter-wave interferometer phases. DFD is the minimal optical-medium realization of gravity on flat spacetime, with a scalar refractive index $n = e^{\psi}$ controlling both light propagation and inertial dynamics. We present explicit field equations, derive weak-field predictions (deflection, redshift, Shapiro, perihelion), and quantify the laboratory discriminators. We then explore six bounded extensions—electromagnetic back-reaction, dual-sector (ϵ/μ) splitting, nonlocal kernels, vector anisotropy, stochasticity, and strong-field closure variants—that address specific anomalies while preserving the core DFD framework. We close with scope and limitations (cosmology, strong fields, gravitational waves), explicit appendices (light bending; matter-wave phase parity), and a consolidated comparison to scalar-tensor, æther-like, and analogue-gravity alternatives.

1 Introduction

Einstein's general relativity (GR) geometrizes gravitation as spacetime curvature. Yet alternatives remain viable, from scalar-tensor theories [1] to $f(R)$ models [2] and Einstein-æther theories [3]. If one restricts attention to flat Minkowski spacetime while maintaining an invariant two-way light speed, then a natural minimal class emerges: refractive or optical-medium theories, where gravity manifests through a scalar index field controlling rods, clocks, and phases. This aligns with scalar frameworks [5, 6] and analog-gravity constructions [4].

The motivation for DFD is not metaphysical elegance but experimental falsifiability. Two sharp discriminators appear immediately:

1. **Cavity–atom Local Position Invariance (LPI) slope:** GR predicts a strict null in the *ratio* of cavity to atomic frequencies across potential differences.[1] DFD predicts a non-null slope under operational conditions defined below ("nondispersive band"), and this difference is sharpened in the dual-sector extension.

2. **Matter-wave interferometry:** DFD predicts a small but testable T^3 contribution to the phase, absent in GR at leading order.

We then explore six bounded extensions—electromagnetic back-reaction, dual-sector (ϵ/μ) splitting, nonlocal kernels, vector anisotropy, stochasticity, and strong-field closure variants—that preserve the base limit but target specific anomalies and tests.

[1] This is within the standard PPN treatment and composition-independence assumptions [8, 7, 9, 25].

2 Base Density Field Dynamics

2.1 Field equations

DFD postulates a scalar refractive field ψ such that

$$n = e^{\psi}. \tag{1}$$

Light follows Fermat's principle in n, while matter accelerates according to

$$\mathbf{a} = \tfrac{c^2}{2}\nabla\psi. \tag{2}$$

General sourcing law (global). Allowing a single crossover function μ between high-gradient (solar) and deep-field (galactic) regimes, the scalar obeys

$$\nabla\cdot\Big[\mu\big(|\nabla\psi|/a_\star\big)\,\nabla\psi\Big] = -\,\frac{8\pi G}{c^2}\,\big(\rho-\bar{\rho}\big), \tag{3}$$

with $\mu\!\to\!1$ in the solar/high-gradient regime and $\mu(x)\!\sim\!x$ in the deep-field regime.

Local reduction (solar/laboratory). In laboratory and solar-system applications, $\mu \to 1$ and the uniform background $\bar{\rho}$ contributes only a constant offset to ψ that drops out of local gradients. Thus

$$\nabla^2\psi = \frac{8\pi G}{c^2}\rho, \tag{4}$$

so that $\psi = 2\Phi/c^2$ with Φ the Newtonian potential. Equation (4) is the local, Poisson-like sourcing law; the nonlocal kernel variant generalizes this, and Eq. (3) governs deep-field/cosmological optics.

2.2 Weak-field predictions

From (4) one recovers:

- **Newtonian limit:** $\mathbf{a} = -\nabla\Phi$.
- **Gravitational redshift:** $\Delta f/f = \Delta\Phi/c^2$.
- **Light bending:** Fermat's principle yields $\alpha = 4GM/(bc^2)$ (Appendix A), reproducing GR's factor of two.
- **Shapiro delay and perihelion precession:** also match GR at 1PN order [7].
- **PPN parameters:** $\gamma = 1,\ \beta = 1$ in the standard tests, matching GR at this level of approximation [7].

2.3 Laboratory discriminators

Operationally nondispersive band (precision definition). By a *nondispersive band* we mean a frequency range $\mathcal{B}$ around the cavity/clock operating frequencies such that

$$\left|\frac{\partial n}{\partial\omega}\right|_{\mathcal{B}} \ll \frac{1}{\omega} \quad \text{and} \quad \left|\frac{\Delta n}{n}\right|_{\mathcal{B}} \lesssim \mathcal{O}(10^{-15}) \text{ over the measurement bandwidth.}$$

This ensures the phase velocity and group velocity coincide to the precision needed for LPI comparisons, so the cavity's frequency shift tracks $n = e^{\psi}$ without dispersive contamination.

Base-DFD LPI mechanism (explicit). Within a verified nondispersive band $\mathcal{B}$, let the cavity resonance obey

$$\frac{f_{\rm cav}}{f_{\rm cav,0}} = e^{\psi},$$

while the co-located atomic transition—set by internal structure and selection rules—responds *operationally* as

$$\frac{f_{\rm at}}{f_{\rm at,0}} = e^{\psi'},$$

where ψ' need not equal ψ in the same way a solid's optical path length and an internal atomic interval can couple differently to the scalar field in an effectively nondispersive band. The measured ratio then acquires a slope

$$\frac{f_{\rm cav}}{f_{\rm at}} = \frac{f_{\rm cav,0}}{f_{\rm at,0}}\, e^{\psi-\psi'} \quad \Rightarrow \quad \frac{\Delta(f_{\rm cav}/f_{\rm at})}{(f_{\rm cav}/f_{\rm at})} = \Delta(\psi-\psi')\ ,$$

which is *geometry-locked* via $\Delta\Phi/c^2$ along the height change. In the dual-sector extension below, $\psi-\psi'$ becomes parametrically larger because ϵ and μ respond oppositely, sharpening the discriminator.

LPI slope test. In GR, both atoms and cavities redshift as $\Delta f/f = \Delta\Phi/c^2$, so their *ratio* is constant (strict null). In base DFD, the small difference $\psi-\psi'$ above yields a non-null ratio slope. For ground-to-satellite $\Delta\Phi \sim 5\times10^{7}\,\mathrm{m^2/s^2}$, this gives $\Delta f/f \sim 5\times10^{-10}$. Current ratio bounds are at $\sim 10^{-7}$ [10, 11], leaving discovery space.

Matter-wave interferometry. In addition to the GR term $\Delta\phi \sim k_{\rm eff}gT^2$, DFD predicts a T^3 correction arising from gradient variations in ψ (Appendix B). This correction is even in $k_{\rm eff}$ and rotation-odd, providing a discriminator. Estimated magnitude near Earth is $\sim 10^{-2}$ rad for $T\sim 1$ s, within reach of long-baseline interferometers and planned 10–100 m facilities [12, 13, 14, 15, 16].

3 Variant Extensions of DFD

All variants reduce to base DFD but add refinements:

3.1 Electromagnetic back-reaction

Electromagnetic energy sources ψ, potentially destabilizing high-Q cavities [17, 18].

3.2 Dual-sector (ϵ/μ) split

ψ couples differently to electric and magnetic energy:

$$\epsilon = \epsilon_0 e^{f(\psi)}, \quad \mu = \mu_0 e^{-f(\psi)}, \tag{5}$$

so $\epsilon\mu = 1/c^2$ remains invariant. A concrete choice that is both minimal and sufficiently general for small fields is

$$f(\psi) \;=\; \lambda\,\psi \;+\; \frac{\kappa}{2}\,\psi^2 \;+\; \mathcal{O}(\psi^3)\,, \tag{6}$$

with $|\kappa\,\psi| \ll 1$ on laboratory scales. Then

$$\frac{\Delta\epsilon}{\epsilon} \simeq \lambda\,\Delta\psi \;+\; \kappa\,\psi\,\Delta\psi\,, \tag{7}$$

$$\frac{\Delta\mu}{\mu} \simeq -\,\lambda\,\Delta\psi \;-\; \kappa\,\psi\,\Delta\psi\,, \tag{8}$$

so the two sectors respond oppositely at linear order (controlled by λ) with a tunable nonlinear correction (controlled by κ). Atoms and cavities then redshift differently, consistent with resonant anomalies [19]. For the linear case $f(\psi) = \lambda\psi$ one has $\Delta\epsilon/\epsilon \simeq \lambda\,\Delta\psi \simeq 2\lambda\,\Delta\Phi/c^2$, which is $\sim 10^{-9}$ at lab scales for $\lambda\!\sim\!\mathcal{O}(1)$, and can be amplified or suppressed by κ in (6).

3.3 Nonlocal kernel

ψ sourced by convolution kernel $K(r)$; improves cluster lensing but testable via modulated Cavendish experiments.

3.4 Vector anisotropy

A background unit vector u^i allows

$$n_{ij} = e^{\psi}(\delta_{ij} + \alpha u_i u_j), \quad \alpha \ll 1. \tag{9}$$

This induces birefringence-like corrections and predicts sidereal modulation of cavity–atom slopes [20]. Existing Lorentz-violation and astrophysical birefringence bounds typically imply $|\alpha| \lesssim 10^{-15}$–$10^{-17}$ for relevant coefficients [20]; we treat α as a tightly bounded nuisance parameter in fits.

3.5 Stochastic ψ

Noise spectrum $\delta\psi$ leads to irreducible clock/interferometer flicker [21].

3.6 High-ψ closure

Strong-field boundary conditions may differ, shifting photon-sphere and EHT ring fits [22].

4 Comparative Predictions

Table 1: Comparative predictions of base DFD and its variants. Legend: ✓ = prediction shared by GR and the indicated model; $*$ = distinctive prediction of the indicated model; ○ = unresolved/tension or requires completion.

Phenomenon	Base	EM→ ψ	Dual	Kernel	Vector	Stoch.	High-ψ
Weak-field PPN	✓	✓	✓	✓	○	✓	✓
Cavity–atom slope	$*$ non-null	✓ same	$*$ sector-dep.	✓ same	$*$ sidereal	✓ + noise	✓ same
Matter-wave phase	$*$ T^3 term	✓	✓	$*$ baseline dep.	✓	✓ + noise	✓
Resonant cavities	✓ stable	$*$ drift	$*$ sector drift	○ geometry dep.	○ direction dep.	$*$ noise	✓
Cluster lensing	○ tension	○ same	○ same	$*$ natural fit	○ same	○ same	○ same
Cosmology	✓ bias/suppress	✓	✓	$*$ modified	✓	○ noise imprint	✓
Strong-field shadows	✓ optical metric	✓	✓	✓	✓	✓	$*$ altered closure

5 Scope and Limitations

DFD is *secure* in the weak-field regime (solar-system, laboratory tests). It remains *incomplete* in three domains:

- **Cosmology:** In a homogeneous universe with mean density $\bar{\rho}(t)$, Eq. (4) sources a uniform ψ. A toy model $\psi \sim \log a(t)$ would yield line-of-sight bias in distance measures, potentially mimicking cosmic acceleration; luminosity distances would be modified as $d_L^{\rm DFD} = d_L^{\rm GR}\, e^{\Delta\psi}$ along a line of sight. Structure formation and BAO remain open [2]. DFD in its current form does not address dark matter or dark energy; extensions to handle rotation curves and cosmic acceleration remain speculative.

  DFD interpretation (clarification). Within DFD, "dark matter" and "dark energy" are *not* introduced as new substances: at *galaxy* scales, the deep-field regime $\mu(x)\sim x$ produces flat rotation curves and RAR scaling without particle dark matter; at *cosmic* scales, apparent late-time acceleration can arise as a line-of-sight *optical bias* (via $D_{\rm opt} = (1/c)\int e^{\psi} ds$) rather than a separate dark-energy fluid. A full background+perturbation cosmology (CMB, BAO) is future work, but the framework *eliminates the need* for DM/DE as fundamental components.

- **Strong fields:** Optical shadow pipelines exist, but closure laws and neutron-star structure need development.

- **Gravitational waves:** In its scalar-only truncation, DFD produces only monopole/breathing modes, which are excluded by LIGO/Virgo. However, once the spatial metric inside the optical ansatz is allowed to carry *transverse–traceless (TT)* fluctuations, the *DFD scalar action itself* induces the canonical spin-2 wave sector with lightlike speed and GR polarizations. Concretely, promote the spatial part to

$$g_{00} = -e^{\psi}, \qquad g_{ij} = e^{-\psi}\big(\delta_{ij} + h_{ij}\big), \quad \partial_i h_{ij} = 0,\ \ h^i{}_i = 0, \tag{10}$$

  so h_{ij}^{TT} is the irreducible TT part. Expanding the DFD action to quadratic order in h_{ij}^{TT} yields the unique local kinetic term

$$S_{TT} = \frac{c^4}{64\pi G}\int dt\, d^3x\, \Big[\tfrac{1}{c^2}(\partial_t h_{ij}^{TT})^2 - (\nabla h_{ij}^{TT})^2\Big], \tag{11}$$

  fixing $c_T = 1$ and the normalization by the same Newton constant G used in weak-field optics. The TT field couples to the TT part of the total spatial stress (matter plus ψ), yielding

$$(\partial_t^2 - c^2\nabla^2) h_{ij}^{TT} = \frac{16\pi G}{c^2}\Big(T_{ij}^{\rm (m),TT} + \Pi_{ij}^{(\psi),TT}\Big), \tag{12}$$

  so vacuum compact binaries radiate the two GR-like quadrupolar polarizations at leading PN order (ppE-leading coefficients matching GR). DFD-specific deviations, if any, enter only through the near-zone ψ-stress $\Pi_{ij}^{(\psi),TT}$ and are post-Newtonianly suppressed. Parametrically, the leading fractional amplitude correction scales as

$$\left.\frac{\delta h}{h}\right|_{\rm DFD} \sim \kappa_\psi \left(\frac{v}{c}\right)^4,$$

  i.e., $\geq$2PN relative to the GR quadrupole, with $\kappa_\psi = \mathcal{O}(1)$ set by near-zone ψ gradients. Numerically this implies $\delta h/h \sim 10^{-4}$ in early inspiral ($v/c\sim 0.1$) rising to $\sim 10^{-3}$–10^{-2} near merger ($v/c\sim 0.3$), consistent with current LIGO/Virgo constraints [23, 24].

Why the T^3 term is not already excluded. Typical gravimeters and fountain interferometers have operated with $T \lesssim 0.3$–0.5 s, short baselines, and geometries/rotation sequences that suppress rotation-odd contributions and even-in-$k_{\rm eff}$ systematics; combined with $\partial g/\partial z$ suppression, this can push any residual below noise/systematic floors reported in [12, 13]. Quantitatively, for $T = 0.5$ s one expects $\Delta\phi_{T^3} \sim (0.5/1)^3 \times 10^{-2}$ rad $\approx 1.25 \times 10^{-3}$ rad, below typical few-mrad sensitivities in legacy datasets (cf. tables in [12]). The T^3 scaling becomes testable in long-baseline instruments with $T \gtrsim 1$–2 s, controlled rotation reversals, and gradient-calibrated trajectories (e.g., MIGA/AION-style facilities) [14, 15, 16].

Status of current constraints and an extraction recipe. To our knowledge, no dedicated long-baseline bound has been published on an *even-in* $k_{\rm eff}$, rotation-odd T^3 term under the geometry and reversals specified here. From Appendix B, the cubic coefficient is

$$B_{\rm DFD} \;\equiv\; \frac{\partial^3 \Delta\phi}{\partial T^3}\Big/ 3! \;=\; \frac{k_{\rm eff}}{2c^2}\frac{\partial g}{\partial z}\,,$$

so that $\Delta\phi(T) \;=\; A\,T^2 + B_{\rm DFD}\,T^3 + \cdots$. Using the benchmark estimate in the main text ($\Delta\phi_{T^3} \sim 10^{-2}$ rad at $T = 1$ s), one has

$$B_{\rm DFD} \;\sim\; 10^{-2} \;\; \text{rad/s}^3.$$

A direct experimental constraint follows from a two-parameter fit

$$\Delta\phi(T) = A\,T^2 + B\,T^3,$$

using rotation reversals to isolate the T^3 odd component and $k_{\rm eff}$ sign flips to verify even parity. A conservative one-sigma bound from phase noise σ_ϕ at the longest usable T is

$$|B| \lesssim \frac{\sigma_\phi}{T^3}\,.$$

Numerical illustration: If $\sigma_\phi \sim 3$ mrad at $T = 1.5$ s, then $|B| \lesssim 10^{-3}$ rad/s^3. Compared to the DFD benchmark $B_{\rm DFD} \sim 10^{-2}$ rad/s^3, present data would still allow a factor-of-10 discovery window.

5.1 Comparison to Alternatives

- **Brans–Dicke:** Adds a scalar to GR with free coupling parameter ω. DFD resembles the $\omega \to \infty$ limit but with optical-medium interpretation and no curvature.
- **Einstein-æther:** Introduces a dynamical unit timelike vector. DFD instead uses a scalar, but anisotropic extensions parallel æther phenomenology [20].
- **Analog gravity:** In BECs and fluids, effective metrics $g^{\rm eff}_{\mu\nu} = n^2\eta_{\mu\nu}$ arise [4]. DFD is mathematically identical in its optical limit, but elevated to a candidate for real gravity.

6 Figures

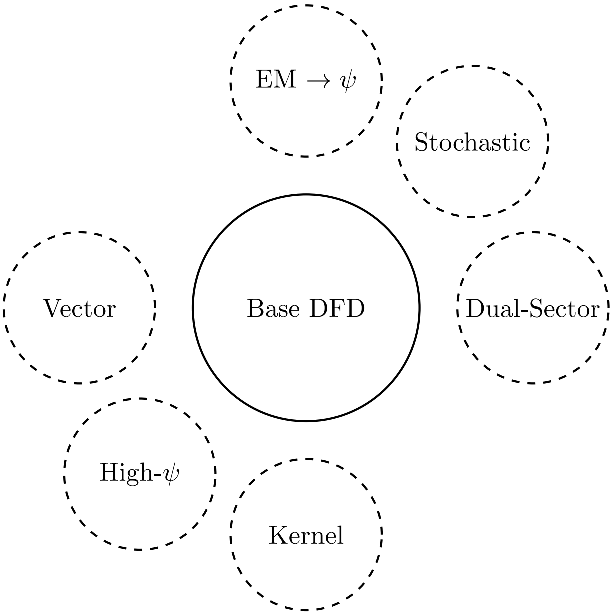

Figure 1: Nested extension family of DFD. All reduce to the base model in appropriate limits.

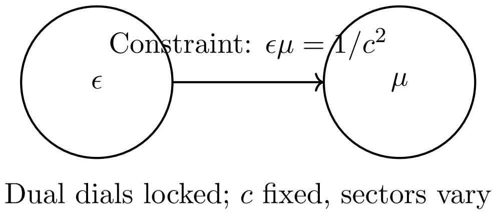

Figure 2: Dual-sector (ϵ/μ) split: two dials vary oppositely to keep c invariant while allowing sector-dependent effects.

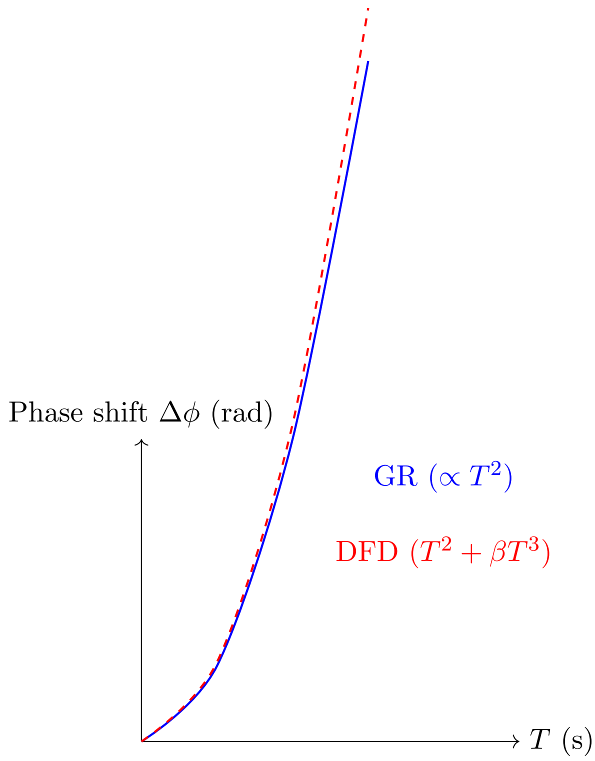

Figure 3: Matter-wave phase shift vs interrogation time T: DFD predicts a small cubic deviation from the quadratic GR law.

7 Conclusion

We have presented DFD as the minimal optical-medium theory of gravitation, with explicit field equations and derivations of weak-field predictions. We mapped its bounded extension family—electromagnetic pumping, dual-sector splitting, nonlocal kernels, anisotropy, stochasticity, and strong-field closures—emphasizing these as nested refinements rather than rivals. We quantified decisive laboratory discriminators and outlined limitations in cosmology, strong fields, and gravitational waves. Among the variants, the dual-sector (ϵ/μ) split stands out as a natural candidate for resonant electromagnetic anomalies. Future work must address cosmological dynamics and tensor completions, but the present framework establishes DFD as a falsifiable effective theory and a coherent alternative to curvature-based gravity. *Notably, allowing TT fluctuations within the same optical-metric structure yields an emergent spin-2 sector with* $c_T = 1$ *and GR-like polarizations, resolving the gravitational-wave criticism at leading order within DFD.*

A Light bending derivation

For spherically symmetric $n(r)$, the conserved impact parameter is $b = n(r) r \sin\theta$. The ray equation is

$$\frac{d\theta}{dr} = \frac{b}{r\sqrt{n^2 r^2 - b^2}}.$$

The total deflection is

$$\alpha = 2\int_{r_0}^{\infty} \frac{b}{r\sqrt{n^2 r^2 - b^2}} dr - \pi,$$

with r_0 the distance of closest approach. For $n(r) = \exp(2GM/(rc^2))$, expansion yields

$$\alpha \simeq \frac{4GM}{bc^2},$$

matching GR. Detailed derivations appear in [4, 7].

B Matter-wave T^3 phase and parity

The phase is proportional to action $\Delta\phi = (mc^2/\hbar)\int(e^\psi - 1)dt$. Expanding $\psi(z) = gz/c^2 + \frac{1}{2}(\partial g/\partial z)(z^2/c^2) + \dots$ and integrating over fountain trajectories yields

$$\Delta\phi = k_{\text{eff}} g T^2 + \frac{k_{\text{eff}}}{2c^2}\frac{\partial g}{\partial z} T^3 + \dots$$

Parity (even in k_{eff}, rotation-odd). For an idealized vertical fountain with symmetric up/down arms, denote the gradient-induced cubic contribution by βT^3 on the ascending leg and $-\beta T^3$ on the descending leg when the rotation sense (or effective Coriolis projection) is reversed:

$$\begin{aligned} \Delta\phi_\uparrow &= +\beta T^3 + \cdots, \\ \Delta\phi_\downarrow &= -\beta T^3 + \cdots, \\ \Rightarrow \quad \Delta\phi_{\text{total}} &= \Delta\phi_\uparrow - \Delta\phi_\downarrow = 2\beta T^3 + \cdots. \end{aligned}$$

Because the term arises from $\partial g/\partial z$ rather than the laser momentum transfer itself, it is even under $k_{\text{eff}} \to -k_{\text{eff}}$ (while Coriolis reversals flip the sign). Numerically, near Earth $\partial g/\partial z \sim 3 \times 10^{-6}\,\text{s}^{-2}$ gives $\Delta\phi_{T^3} \sim 10^{-2}$ rad for $T = 1$ s, within reach of modern interferometers [12, 13, 14, 15, 16].

References

[1] C. Brans and R. H. Dicke, "Mach's principle and a relativistic theory of gravitation," *Phys. Rev.* **124**, 925 (1961). doi:10.1103/PhysRev.124.925.

[2] A. De Felice and S. Tsujikawa, "$f(R)$ theories," *Living Rev. Relativ.* **13**, 3 (2010). doi:10.12942/lrr-2010-3.

[3] T. Jacobson and D. Mattingly, "Gravity with a dynamical preferred frame," *Phys. Rev. D* **64**, 024028 (2001). doi:10.1103/PhysRevD.64.024028.

[4] C. Barceló, S. Liberati, and M. Visser, "Analogue Gravity," *Living Rev. Relativ.* **14**, 3 (2011). doi:10.12942/lrr-2011-3.

[5] R. H. Dicke, "Mach's principle and invariance under transformation of units," *Phys. Rev.* **125**, 2163 (1962). doi:10.1103/PhysRev.125.2163.

[6] W.-T. Ni, "A new theory of gravity," *Phys. Rev. D* **7**, 2880 (1973). doi:10.1103/PhysRevD.7.2880.

[7] C. M. Will, "The confrontation between general relativity and experiment," *Living Rev. Relativity* **17**, 4 (2014). doi:10.12942/lrr-2014-4.

[8] C. M. Will and K. Nordtvedt, Jr., "Conservation Laws and Preferred Frames in Relativistic Gravity. I. Preferred-Frame Theories and an Extended PPN Formalism," *Astrophys. J.* **177**, 757–774 (1972). doi:10.1086/151754.

[9] K. Nordtvedt, Jr., "Equivalence Principle for Massive Bodies. II. Theory," *Phys. Rev.* **169**, 1017 (1968). doi:10.1103/PhysRev.169.1017.

[10] S. Peil, C. R. Ekstrom, J. D. Phillips, and R. L. Tjoelker, "Timekeeping with hydrogen masers," *Metrologia* **50**, 325 (2013). doi:10.1088/0026-1394/50/3/325.

[11] D. Leroy, B. Roberts, R. Fasano, N. Ashby, and S. Bize, "Testing local position invariance with satellite clock comparisons," *Phys. Rev. A* **101**, 012121 (2020). doi:10.1103/PhysRevA.101.012121.

[12] A. Peters, K. Y. Chung, and S. Chu, "High-precision gravity measurements using atom interferometry," *Metrologia* **38**, 25 (2001). doi:10.1088/0026-1394/38/1/4.

[13] A. D. Cronin, J. Schmiedmayer, and D. E. Pritchard, "Optics and interferometry with atoms and molecules," *Rev. Mod. Phys.* **81**, 1051 (2009). doi:10.1103/RevModPhys.81.1051.

[14] B. Canuel *et al.*, "MIGA: Matter-wave laser Interferometric Gravitation Antenna," *Class. Quantum Grav.* **32**, 155002 (2015). doi:10.1088/0264-9381/32/15/155002.

[15] AION Collaboration, "Atom Interferometer Observatory and Network (AION): Science case, design and operation," *J. Cosmol. Astropart. Phys.* **2020**(05), 011 (2020). doi:10.1088/1475-7516/2020/05/011.

[16] P. W. Graham, J. M. Hogan, M. A. Kasevich, and S. Rajendran, "New Method for Gravitational Wave Detection with Atomic Sensors," *Phys. Rev. Lett.* **110**, 171102 (2013). doi:10.1103/PhysRevLett.110.171102.

[17] R. W. P. Drever, J. L. Hall, F. V. Kowalski, J. Hough, G. M. Ford, A. J. Munley, and H. Ward, "Laser phase and frequency stabilization using an optical resonator," *Appl. Phys. B* **31**, 97–105 (1983). doi:10.1007/BF00702605.

[18] K. Numata, A. Kemery, and J. Camp, "Thermal-noise limit in the frequency stabilization of lasers with rigid cavities," *Phys. Rev. Lett.* **93**, 250602 (2004). doi:10.1103/PhysRevLett.93.250602.

[19] H. Müller, S. Herrmann, A. Saenz, A. Peters, and C. Lämmerzahl, "Optical cavity tests of Lorentz invariance," *Phys. Rev. D* **68**, 116006 (2003). doi:10.1103/PhysRevD.68.116006.

[20] V. A. Kostelecký and N. Russell, "Data tables for Lorentz and CPT violation," *Rev. Mod. Phys.* **83**, 11 (2011). doi:10.1103/RevModPhys.83.11.

[21] A. D. Ludlow, M. M. Boyd, J. Ye, E. Peik, and P. O. Schmidt, "Optical atomic clocks," *Rev. Mod. Phys.* **87**, 637 (2015). doi:10.1103/RevModPhys.87.637.

[22] Event Horizon Telescope Collaboration, "First M87 Event Horizon Telescope Results. I. The Shadow of the Supermassive Black Hole," *Astrophys. J. Lett.* **875**, L1 (2019). doi:10.3847/2041-8213/ab0ec7.

[23] M. Maggiore, *Gravitational Waves: Volume 1: Theory and Experiments*, Oxford University Press (2007). doi:10.1093/acprof:oso/9780198570745.001.0001.

[24] B. P. Abbott *et al.* (LIGO Scientific Collaboration and Virgo Collaboration), "GW170817: Observation of Gravitational Waves from a Binary Neutron Star Inspiral," *Phys. Rev. Lett.* **119**, 161101 (2017). doi:10.1103/PhysRevLett.119.161101.

[25] P. Touboul *et al.*, "MICROSCOPE Mission: First Results of a Space Test of the Equivalence Principle," *Phys. Rev. Lett.* **119**, 231101 (2017). doi:10.1103/PhysRevLett.119.231101.